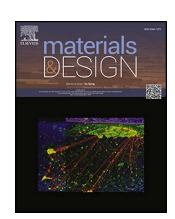
ELSEVIER

Contents lists available at ScienceDirect

# Materials & Design

journal homepage: www.elsevier.com/locate/matdes



# Direct restoration of erosive tooth wear using biomimetic composite and ultrafast laser processing: An in-situ study

Sarathkumar Loganathan <sup>a,\*</sup>, Sandeep Kumar <sup>b</sup>, Simon Strafford <sup>a</sup>, Geeta Sharma <sup>a</sup>, Evangelos Daskalakis <sup>a</sup>, Eric Kumi Barimah <sup>a</sup>, Neelam Iqbal <sup>a</sup>, Anna Neilson <sup>b</sup>, Brian Nattress <sup>b</sup>, Sue Pavitt <sup>b</sup>, El M Raif <sup>b</sup>, Animesh Jha <sup>a</sup>

#### ARTICLE INFO

#### Keywords: Femtosecond laser Tissue surface engineering Restorative bio-composite Direct restoration Erosive tooth wear

#### ABSTRACT

The prevalence of irreversible erosive tooth wear (ETW) results in progressive loss of tooth surface, leading to compromised chewing and mastication functions. The study evaluates the restorative efficacy of a bio-composite for treating the ETW. The in vitro and in situ experiments focused on evaluating the biocompatibility of a laser-assisted bio-composite restoration for eroded enamel surfaces and its potential for in situ saliva remineralisation. The bio-composite was formulated by mixing Fe<sup>3+</sup> doped fluorapatite (FAP) with chitosan hydrogel for restoring artificially created  $\sim 70~\mu m$  deep eroded human enamel lesion. The surface of the restored lesion was then irradiated with a 1040 nm ultrafast laser to densify the material and enhance its bonding with the vicinal healthy enamel

The in-situ appliance study of in-vitro restored lesion was conducted in the selected healthy volunteer's mouth to ascertain and compare the statistical efficacy with the acid-resistant properties of natural human enamel as a control. The in-situ evaluation study demonstrated that the use of ultrafast laser-assisted bio-composite restores lesions and has the potential to prevent further acid erosion. This study also reveals a conceptual remineralisation strategy for effective enamel repair in clinical practices. It offers potential insights into the mechanisms of biomineral formation, thus preventing enamel erosion, which might be implemented for the restoration of human and pet animal tooth wear.

#### 1. Introduction

Erosive tooth wear (ETW) is an oral condition, leading to an incremental irreversible loss of dental enamel which compromises food and beverage intake. ETW has a multifactorial aetiology and can occur due to acid exposure from intrinsic (gastroesophageal reflux disease, hiatus hernia and nausea) or extrinsic factors (beverages, fruits, tobacco, and occupational acidic exposure) [1,2]. People with a prolonged prevalence of ETW may encounter dentin hypersensitivity (DH), tooth shortening, functional tooth damage and discolourations [3,4]. A substantial correlation has been identified between ETW and poor oral health-related quality of life among patients. Several studies have reported that the prevalence of ETW affects 2 to 100 % of adults across the globe [5,6]. It has been growing with increasing age groups. The advancement of ETW leads to exposure of dentin tubules and pulp exposure necessitating

restorative treatments [7,8]. Considering the severity of ETW, several efforts have been made to develop strategies for preventing and minimising enamel and dentin surface erosion. Regardless of etiological causes, current techniques for preventing ETW focus on adhesive protocols and biomimetic methods [2]. They consist of fluoride-based antiacid filler materials (mouthwash, toothpaste, bioactive polymers, varnishes, and gels) that promote globular CaF<sub>2</sub> like precipitates on enamel for preventing demineralisation and encouraging remineralisation in acidic environments. However, long-term exposure to excessive fluoride can cause chronic fluorosis symptoms (dental fluorosis, osteofluorosis, muscle weakness, and low haemoglobin levels) [3]. Numerous remineralisation treatments with different mechanisms of action are available on the market, but the most efficient treatment remains unidentified [2,5]. Besides oral health-related needs for dental care, there is also demand for cosmetic dentistry to improve aesthetic appearance

E-mail addresses: s.loganathan@leeds.ac.uk, saratloganathan@gmail.com (S. Loganathan).

<sup>&</sup>lt;sup>a</sup> School of Chemical and Process Engineering, University of Leeds, Leeds LS2 9JT, UK

<sup>&</sup>lt;sup>b</sup> School of Dentistry and Leeds Dental Hospital, University of Leeds, Leeds LS2 9LU, UK

<sup>\*</sup> Corresponding author.

[6,9]. Depending on the type of tooth damage and appearance, there is also a need for additional preventive techniques in restorative dentistry to provide more effective treatments.

Drawing ideas from nature is a promising strategy for developing safe, sustainable, and effective treatment for ETW. Biomineralisation is a natural process involving a harmony between organic (amelogenin, collagen fibrils) and inorganic elements (hydroxyapatite (HAP), amorphous calcium phosphate (ACP)) [8,10]. Although natural biomineralisation utilises an organic-inorganic composite framework, most contemporary research focuses on mimicking the organic structure, overlooking the provision of inorganic mineral sources (e.g., ACP, HAP) [11,12]. Currently, the research has focused on human amelogenin, peptide analogs and biomacromolecules (polydopamine and chitosan) with protein coating that may induce biomineralisation, offering a promising solution for ETW treatment [8,13]. However, the limited availability of Ca<sup>2+</sup>/Ca<sup>3+</sup> ions in the oral cavity remains a challenge, leading to procrastinated mineralisation that is not commensurate with daily fluctuations in oral saliva pH [8]. Therefore, establishing dental restoration with rapid integration of inorganic minerals and mineralisation-promoting coating might provide an effective treatment

In clinical practice, the precise filling of demineralised regions of dental hard tissues with dental restorative materials in fluid form is deemed difficult. An effective stabilisation technique is required since the new biomimetic materials must thoroughly infiltrate damaged regions [13,14]. The emergence of dental lasers (Er:YAG, Er,Cr:YAG, CO<sub>2</sub>, Nd:YAG, Diode lasers, etc.,) have already been tested with various laser parameters (wavelength, laser power, pulse energy, repetition rate, interaction time and mode of operation) for controlling ETW through chemical compositional alteration [3,15,16]. Numerous studies have demonstrated that the photobiomodulation effect of lasers on dental hard tissues considerably prevents and controls ETW by reducing enamel solubility and permeability [2,17]. Although the prolonged interaction time of conventional lasers (pulse duration > ns) leads to side effects such as collateral damage and necrosis that impede photobiomodulation effects, ultrafast laser technology (pulse duration < a few fs) resolves this issue by precisely confining laser energy to the interaction region with shorter interaction time [18,19]. While ultrafast lasers are predominantly used for hard tissue ablation (photoablation), it is feasible to alter the chemical composition of target tissue via photobiomodulation by controlling the laser parameters at the sub-ablation threshold. Casarin et al. [20] found that irradiating dental hard tissues with an ultrafast laser at sub-ablation parameters dramatically decreased carbonate content while preserving surface morphology (no thermal damage and micro-cracks). Our previous investigations also reported the use of ultrafast lasers in the resonant regime of interaction for reducing thermal load by using high repetition rates in the MHz to GHz regime at 1040 nm Yb<sup>3+</sup>-ion doped solid-state fs lasers [21,22]. Thus, integrating ultrafast laser technology with biomimetic restorative materials that are compatible with the structural and mechanical properties of the surrounding natural tissues may offer a promising solution for ETW by stabilising the materials on eroded surfaces.

This study proposes an ultrafast laser-assisted restoration of the ETW using an organic matrix-inorganic composite. Chitosan, a commonly used cationic polysaccharide-based mucoadhesive, was mixed with the calcium fluorapatite nanoparticles (Fe-doped FAP), which serve as a base filler material and calcium source for ETW restoration. Since chitosan plays a dual role in stabilising the Fe-doped FAP and forming disulfide bonds with glycoproteins, an amyloid-like organic–inorganic matrix composite is ultimately formed. The surface of the applied biocomposite layer was then irradiated with an ultrafast laser (1040 nm) to densify the material and enhance its bonding with the eroded enamel. The in-situ mouth appliance study of the in-vitro laser-assisted restored enamel samples was conducted in the volunteer's mouth to assess the procedure's statistical efficacy and to compare the acid-resistant properties with those of natural enamel samples as a control. The in-situ

evaluation study demonstrated that enamel restored using the proposed direct restoration technique with an ultrafast laser remained stable in the oral environment and showed significant clinical potential for effectively preventing ETW.

#### 2. Materials and methods

#### 2.1. Tooth sample preparation

Human molars were obtained from the tissue bank at the Leeds Dental School following ethical approval from the Dentistry Research Ethics Committee (DREC) for the use of human teeth (200318/JT/246). The teeth were sterilised overnight by incubation in 12 % hypochlorite, followed by 24 h of immersion in PBS [13]. Subsequently, the teeth samples were exposed to gamma radiation at 4080 Gy, a dosage proven to ensure sterilisation without affecting the structural integrity of the enamel [23]. The enamel blocks (~3 mm thickness) were sliced from human molars using a diamond wire saw. The surface of each block was ground to remove the natural curvature of the enamel surface using silicon carbide abrasive paper (grit sizes #600, #1200, and #2000) in the presence of water. The ground surfaces were then polished using alumina paste with grain sizes of 5 µm and 1 µm. Afterwards, the enamel slabs were ultrasonicated in methanol and distilled water to remove abrasive and polishing debris and then stored in artificial saliva to prevent denaturing.

#### 2.2. Preparation of the erosive tooth wear on the enamel surface

The prepared flat enamel surfaces (3  $\times$  3 mm<sup>2</sup>) were masked with nail varnish (Max Factor "Glossfinity"), exposing a 1 mm wide central section on each cusp (Fig. 1). The blocks were then exposed to 1 vol% citric acid solution (pH 3.2, room temperature, 24 h) to cause acid erosion until the exposed area showed a surface loss of approximately 70  $\mu$ m in depth.

# 2.3. Preparation of bio-composite and restoration of erosive tooth wear

Hydroxyapatite nanoparticles doped with 1 mol.%  $Fe^{3+}$  ions were synthesized using the precipitation method as detailed in a previous study [21]. The bio-composite was prepared by homogeneously mixing 0.3 g of  $Fe^{3+}$ -doped FAP with 20 ml of a chitosan solution (0.1 g of chitosan powder dissolved in 20 ml of 1 vol% aqueous acetic acid) under continuous stirring at room temperature. A thin layer of bio-composite coating was applied to the surface of each previously created enamel erosion lesion using a single-channel micropipette and dried at room temperature for 10 min. It was observed that the dried coating was adherent to the surface of the acid-eroded lesion.

# 2.4. Ultrafast laser processing of bio-composite coating

The coated layer was irradiated with an ultrafast laser to densify the coating and enhance its bonding with the underlying enamel. A 1040 nm, 200 fs, 100 MHz Yb-doped femtosecond fibre laser (Chromacity, Edinburgh, UK) was used to irradiate the bio-coating. This laser system can deliver a maximum average power of 2 W with Gaussian spatial distributions and be controlled using a variable attenuator.

A hollow-core fibre (1 m in length) was used to deliver laser energy to the lesion site. The coated dental enamel ( $\sim$ 1.2 mm thickness) was loaded on a high-precision CNC-controlled XYZ stage (100 nm resolution). Laser irradiation on bio-composite coating was performed using a 15 mm focal lens with the laser beam focused perpendicular to the coated surface through an automatic focusing CCD camera (Fig. 1). The coated layer was scanned with laser over  $1.2 \times 2 \text{ mm}^2$  areas by adopting single-line scanning techniques (5 mm/s) with the hatch distance of 50  $\mu$ m at an average laser power of 530 mW [21]. The dental samples were grouped into two categories: Group 1 (single layer) and Group 2 (double

Fig. 1. Direct dental restoration of erosive tooth wear: in-situ study.

layer) based on the coating procedure used for enamel erosion. In group 2, a second layer was applied to enhance the surface finish and compensate for shrinkage caused by the laser.

#### 2.5. Characterisation

The surface morphology analysis was carried out at each stage of the dental restoration process, which included producing the ETW on dental enamel, restoring the ETW with composites and densification using laser irradiation. The microstructural properties and dimensions of the enamel surface were analysed using a Proscan profilometer and SEM (Hitachi TM3030Plus). This process was then repeated after the in situ experimental period to assess any changes in the surface losses. The chemical composition of the restored enamel was analysed using Raman and energy-dispersive spectroscopy (EDS) analysis.

# 2.6. In vitro cytotoxicity, cell culture and remineralisation study

Cytotoxicity of bio-composites was evaluated using a colorimetric assay, MTT (3-(4,5-dimethylthiazol-2-yl)-2,5-diphenyltetrazolium bromide) with A549 cells and Alamar Blue with human primary periodontal cells according to the manufacturer's instructions (Sigma-Aldrich). A549 Cells were obtained from the tissue bank (Ref No. 200318/JT/ 246) and periodontal cells were isolated from extracted teeth obtained from the Leeds Dental School (Ref No. 160418/SK/248). A549 cultured using DMEM high glucose (Sigma-Aldrich, Life Science) and periodontal cells were cultured using low glucose DMEM (Sigma-Aldrich, Life Science) cell culture media supplemented with 10 % FBS, 1 % L-glutamine, and 1 % penicillin-streptomycin. The cells (1x10<sup>4</sup> cells per/cm<sup>2</sup>) were cultured over restored bio-composite  $(1.2 \times 2 \text{ mm}^2)$  that were cleaned and sterilized in advance by immersing into 70 vol% ethanol (2 h) and by subsequent UV exposure (20 min each surface). The cultured cells were maintained under aseptic conditions in a CO<sub>2</sub> incubator at 37 °C, in air containing 5 % CO2 and at a 95 % relative humidity. Cytotoxicity assessment of the bio-composite was performed by measuring fluorescence at 450 nm using a Varioskan Flash plate reader (Thermo Scientific). The laser confocal microscopy was performed to analyze the qualitative cytotoxicity (live/dead) and to visualise the cell adhesion (Alexa Flour 488 and DAPI, Sigma Aldrich) over the bio-composite using a Leica TCS SP2 confocal laser scanning microscope. Furthermore, cells cultured over the laser-irradiated bio-composite were visualised using SEM (TM3030 plus), and the internalisation of Fe-doped FAP biocomposite nanoparticles in the cells was observed using TEM (Fig. 3) as reported earlier [24]. The elemental composition (EDS) confirmed the chemical composition of internalised bio-composite material. The remineralisation potential of the restored ETW lesions in artificial saliva was evaluated using Raman Spectroscopy, X-ray diffraction (XRD) (Empyrean), Nano-indentation (Berkovic intender) and cross-sectional SEM-EDS analysis.

#### 2.7. Design of in-situ study

An in-situ human study (Fig. 2) was conducted to evaluate the protection of laser-assisted restored eroded enamel (lesion depth of 60–90  $\mu m$ ) with an appetite-like biomimetic composite (experimental) in the oral environment.

The study consisted of human enamel slabs with laser-densified composite coating and unfilled lesions (control) mounted on a dental

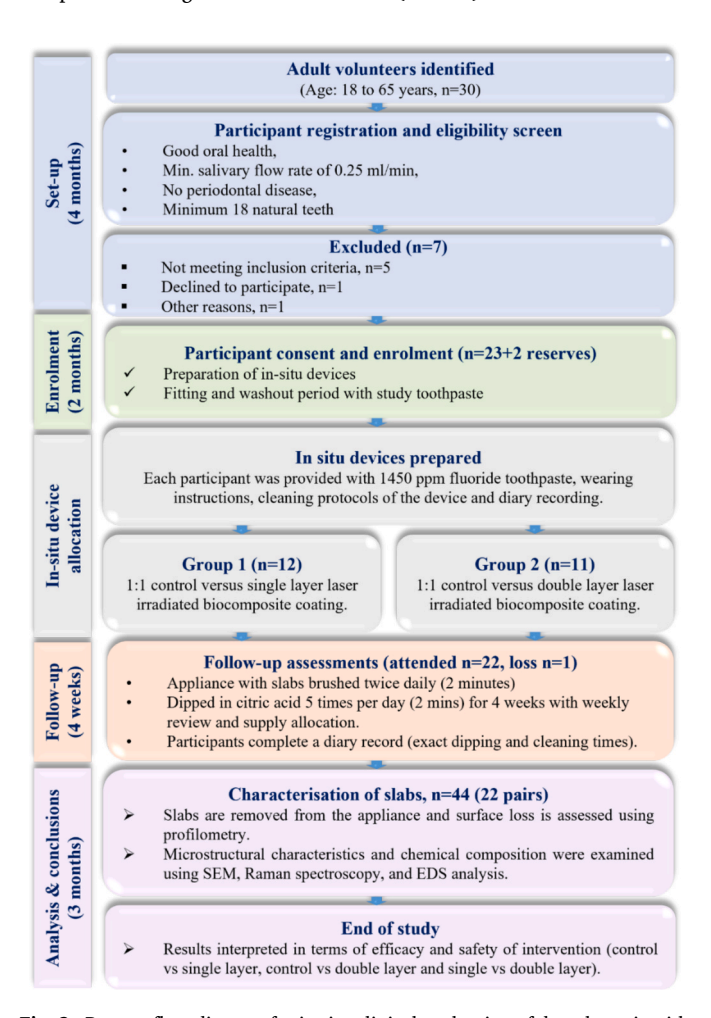


**Fig. 2.** Process flow diagram for in situ clinical evaluation of dental repair with ultrafast laser technology.

appliance and tested under an erosive challenge in the volunteer's mouth. Ethical approval for this study is sought from the DREC, University of Leeds (DREC reference number: 200318/JT/246). A participant is considered enrolled in the study after they have signed and witnessed the informed consent form. This study is conducted in full conformance with the laws and regulations of the UK and the Declaration of Helsinki/Venice/Tokyo/Hong Kong/South Africa (1996). Approximately 30 volunteers with satisfactory dental health were screened to identify n=23 participants (plus two reserves) who were enrolled to complete the study. The volunteer's ages range from 18 to 65 years old with most being students and staff from the University of Leeds.

#### 2.7.1. Experimental appliance

A maxillary removable palatal appliance with U-clasps engaging on the upper first permanent molars and an acrylic plate on the palatal surface was a bespoke appliance for each volunteer who participated in the study. The pairs of human enamel lesion slabs prepared earlier were (as in Section 2.1-2.4) secured in the palatal plate of the appliance using a wired dental acrylic device. This arrangement exposed the slabs to the oral environment; however, they were protected from the effect of the tongue using arched wires, leaving a 1 mm gap between the wire and the slabs. This appliance design is widely used to prevent children from thumb-sucking; therefore, it was comfortably accepted by the volunteers (Fig. 1).

# 2.7.2. Acclimatisation period, wash-out period and treatment phase

Initial exposure of the dental appliances to the oral environment can be uncomfortable for volunteers. Hence, the volunteers in this study were provided with an in-situ oral appliance for up to 7 days before commencing the study (i.e., the wash-out phase). During this period, the participant always wore the appliance (except when eating, drinking, or brushing their teeth). If the participant experienced discomfort, they reported back to the clinic to have the appliance adjusted and then continued with the acclimatisation period.

The study treatment phase began with a one-week pre-treatment wash-out period before the split-mouth study, during which participants brushed their teeth with a provided toothbrush and fluoridated toothpaste (1450 ppm). The participants were asked to abstain from additional oral hygiene procedures such as flossing and mouthwash. At the end of the wash-out period of the study, the participants returned the insitu oral appliances to the study site. The appliances were then disinfected and fitted with two slabs (one pair of enamel slabs, i.e., one control and one test) for the treatment phase.

Participants wore the intra-oral upper removable appliance for 4 weeks during the in-situ study. Each volunteer was given a set of prescriptive instructions to follow the procedure. The procedure was repeated daily for 28 days (4 weeks). At the end of the study, the participant left the in-situ intraoral appliance with the clinic. The amount of surface loss was calculated at the end of the 4-week in-situ study period using an objective readout from a light surface profilometry (Proscan Scantron), which measures the depth of the eroded surface.

### 2.7.3. Follow-up period

The volunteers were recalled for a follow-up visit (within 14 days) after the study concluded. The participants were provided with a brief medical interview questionnaire and were assessed clinically for oral health. A professional cleaning was provided when necessary.

# 2.7.4. Statistical analysis

Data analysis was performed over three independent experiments (in vitro and in situ) conducted in triplicate (n = 3). Statistical analysis was performed using IBM SPSS Statistics software (version: 29.0.0.0 (241)) and considered significant if p < 0.05.

#### 3. Results and discussions

# 3.1. Preparation and characterisation of artificial erosive tooth wear on enamel slabs and bio-composite

As stated above, the artificial ETW on human enamel slabs was created by exposing the surface of each enamel slab to a 1 vol% citric acid solution (pH 3.4) for 24 h to obtain a lesion depth comparable to natural ETW. Fig. 3f shows a typical surface profile of the artificial ETW lesion obtained using a Proscan surface profiler. The depth was measured from the baseline (masked zone in Fig. 1) as a reference. An average lesion depth on enamel slabs was found to be  $70.2 \pm 7.41 \ \mu m$ .

The particle size analysis of the bio-composite was performed using a Malvern Zetasizer, and the resulting size distribution curve is presented in Fig. 3a. The particles ranged in size from 220 nm to 550 nm, with a mean size of  $\sim 350$  nm. The particle size of the inorganic minerals dispersed in a biopolymer (chitosan) matrix plays a critical role in determining the packing density of the paste and its spreading characteristics, which are dependent on the weight fractions of the Fe-doped FAP mineral and chitosan. Empirically, it was found that the spreading characteristic of the paste, determined by the mineral weight fraction, controls the post-laser densification of the mineral inside the lesion. It is essential for the absorbed radiative energy from the laser to be subsequently dissipated in a mineral-packed bed.

Experimental observations also concluded that sub-500 nm mineral particles offered much better adherence to the surrounding enamel surface. We also observed that since the artificial acid erosion yields variable topological surface roughness of the lesion, the sub-500 nm particles offered much better filling around the topology, as can also be verified from the cross-sectional examination of the interface using the SEM.

A complementary part of the mineral adherence with the lesion surface was also carried out by characterising the zeta potential measurements of the colloidal form of biomineral with chitosan. For the surface charge analysis of Fe-doped FAP mineral in a chitosan colloidal mixture, the zeta potential values of mineral, chitosan, and mineralchitosan suspension were characterised. In Fig. 3b, the values of zeta potential of Fe-doped FAP, chitosan, and mineral-chitosan colloidal mixture are compared. The inorganic Fe-doped FAP nanoparticles have a negative surface potential at -16.5 mV, whereas the chitosan solution exhibits a positive zeta potential of + 104 mV. It is because the chitosan is a natural polysaccharide, constituted of randomly dispersed β-linked D-glucosamine and N-acetyl-D-glucosamine units. The presence of amino groups on its surface leads to considerable protonation at neutral pH which is why the chitosan solution yields a positive surface charge. When the mineral particles are dispersed, the equilibrium surface potential is not simply the subtraction of a -16.5 mV charge from a +104mV charge. Still, it appears more complex, with a resulting colloidal mixture zeta potential of + 41.3 mV. The magnitude of the resultant surface charge in the colloidal points indicates the surface functionalisation leading to a stable suspension with little evidence of segregation.

SEM is a valuable tool for examining cell attachment and behaviour on material surfaces, providing high-resolution images of surface topography and cellular morphology. The cell attachment and behaviour of human alveolar basal epithelial cells (A549 cells) on the biocomposite surface were examined using SEM. The analysis of the surface topography and A549 cells morphology cultured on the material shown in Fig. 3e, demonstrates that after 24 h of cell culture, A549 cells were well-adhered and appeared flattened, exhibiting numerous extensions typical of fibroblasts [24,25]. This suggests that the restorative bio-composite provides a favourable environment for cell attachment.

Furthermore, cellular interactions with the bio-composite were assessed using High-Angle Annular Dark Field Scanning Transmission Electron Microscopy (HAADF-STEM). The STEM images in Figs. 3c and d provide visual confirmation of Fe, Ca, and FAP uptake at the individual cell level. In these two TEM images of cell sections, a needle-like

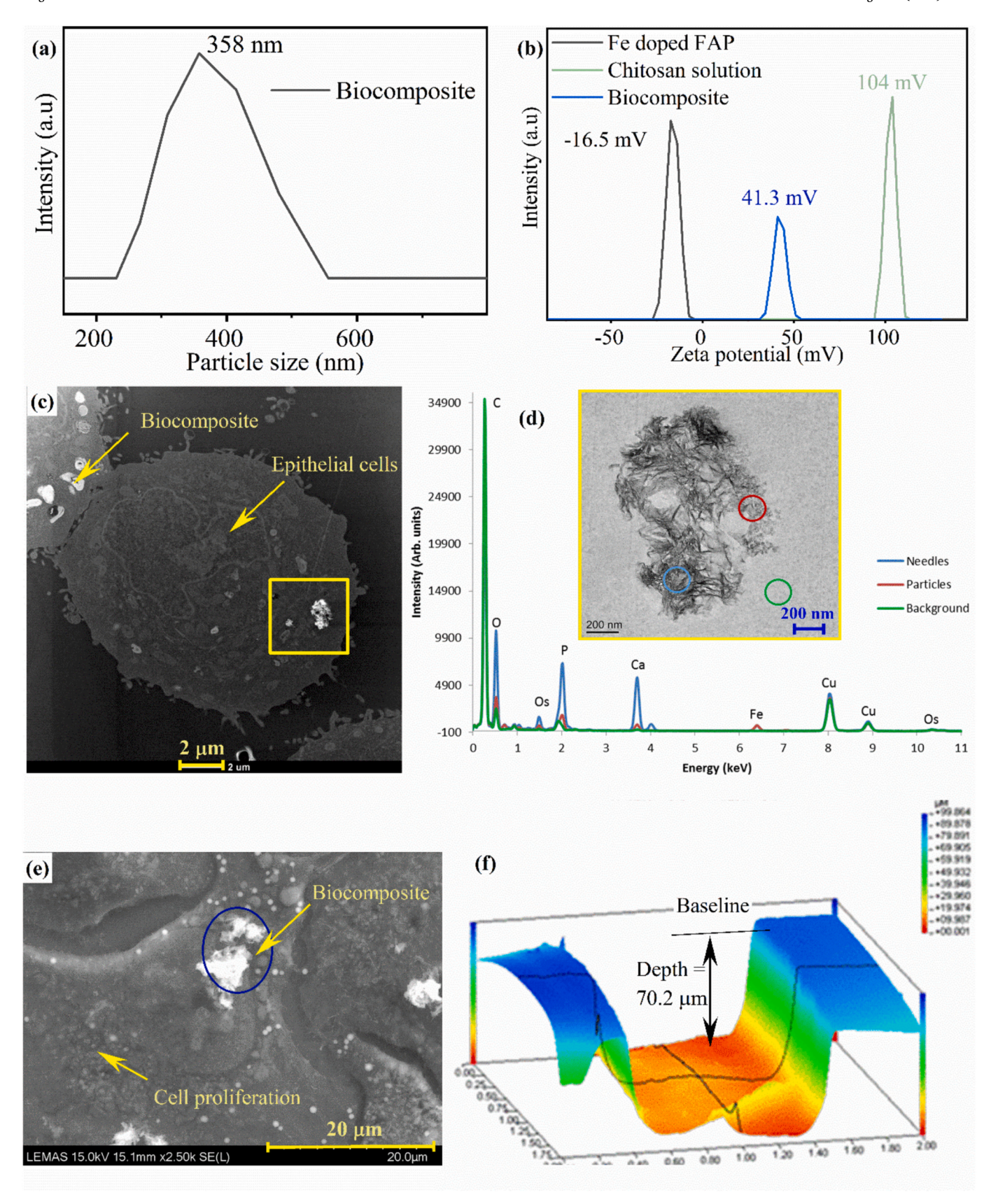


Fig. 3. Analysis of microstructural properties and biocompatibility of restorative bio-composite (a) Particle size distribution of inorganic minerals in bio-composite, (b) Zeta potential measurement to evaluate the stability colloidal bio-composite (c) TEM image of agglomerated Fe-doped FAP nanoparticles internalised in A549 cells (d) EDX analysis confirming the chemical composition of internalised Fe-doped FAP in A549 cell (e) SEM image of cell adhesion study on bio-composite (f) Surface profiler image of artificial ETW on enamel slabs.

structure with a particle size of  $\sim$  180 nm is observed to be internalised in A549 epithelial cells (Fig. 3c).

The internalised material was evident as an agglomeration of faceted electron-dense particles localised within the cytoplasm, consistent with the expected size of the nanoparticles (Fig. 3a). The apparent cellular internalisation of a cluster of needle-shaped minerals was also confirmed as Fe-doped FAP using the EDX analysis (Fig. 3d). The internalised Fe-doped FAP nanoparticles appeared more rod- or needle-like shape which suggests the bio-composite readily interacted with the A549 cell surface. The mechanism of internalisation can be explained based on the lipid cellular wall, which allows ion gating, including Ca<sup>2+</sup> and phosphate ions, necessary for cell viability and mitochondrial function.

# 3.2. Restoration of erosive tooth wear with biomimetic composite using ultrafast laser

The steps involved in the restoration of ETW are: a) filling the lesion surface with a restorative bio-composite, followed by b) densification using ultrafast laser irradiation. To determine the effect of laser irradiation, the surface morphology was measured at two different stages: before laser irradiation and after laser irradiation, as exemplified in Fig. 4a and b, respectively. After filling the restorative bio-composite, the average lesion depth was found to be  $14.78 \pm 3.21~\mu m$  (Fig. 4a). Each filled lesion was then irradiated with an optimised average laser power of 0.53 W (refer to section 4.3). After laser irradiation, the densified mineral increased the average lesion depth to  $29.08 \pm 4.13~\mu m$ , indicating material shrinkage due to laser energy transfer. The increase in the lesion depth after mineral filling and post-laser

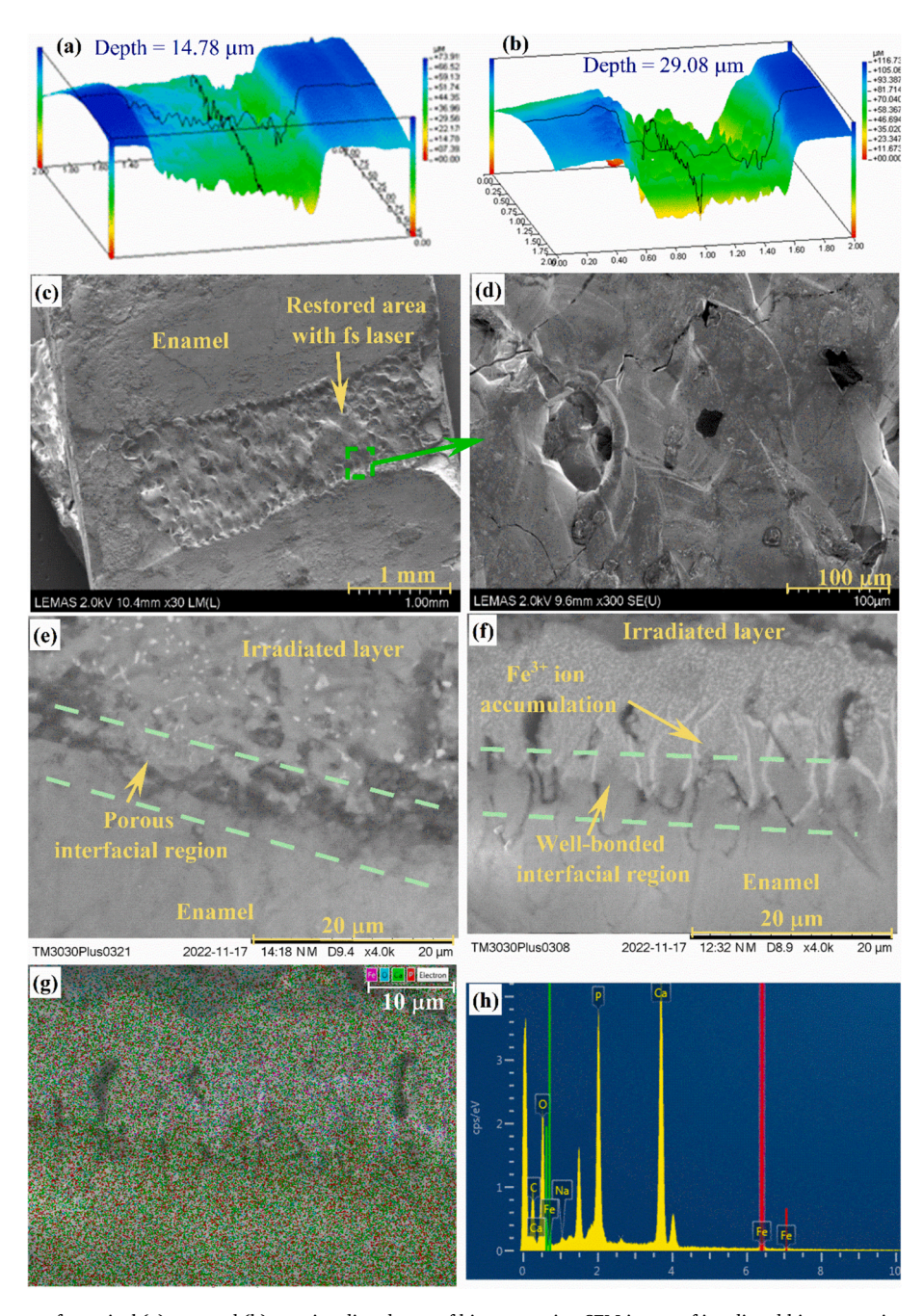


Fig. 4. Surface profiler image of a typical (a) pre- and (b) post-irradiated area of bio-composite. SEM image of irradiated bio-composite coating. (c-d) Restored bio-composite with laser tracks. Cross-sectional SEM images of (e) single layer and (f) double layer coating with (g-h) EDX analysis.

densification suggests that out of 70  $\mu m$  initial lesion depth, nearly 40  $\mu m$  of the lesion was filled with the bio-composite mineral. The remaining unfilled depth of  $\sim 30~\mu m$  was used for fine finish by refilling the lesion with a second layer of bio-composite, followed by laser densification.

The examination of the topological surface after laser densification was carried out using scanning electron microscopy. The SEM topological surface and microstructural images are shown in Figs. 4c and d. Although the low-magnification image in Fig. 4c does not show any evidence of macroscopic cracks arising from thermal stress between the enamel and the irradiated layer, the high-magnification image in Fig. 4d clearly shows the prevalence of microscopic cracks and pores. The origin of the micropores and cracks may have been due to differential radiation absorption due to laser scattering from an optically rough surface and the consequential thermal stress. The formation of microscopic defects requires further investigation so that lesion restoration mimics the natural mineral enamel as closely as possible.

Also, since the double layer of bio-composite is subjected to laser interaction twice, there is expected to be a difference in the coefficient of thermal expansion between the double-layer (anisotropic expansion coefficient:  $\alpha_a=(\pm 0.06)\times 10^{-5}~K^{-1}$  and  $\alpha_c=2.2~(\pm 0.06)\times 10^{-5}~K^{-1})$  and the single-layer due to microstructure changes occurring in bio-composite restoration [26]. It is known from the literature that the difference between the expansion coefficients may be of the order of  $(10^{-1}~K^{-1})$  which may be responsible for microscopic crack formation due to the anisotropic nature of the crystalline lattice.

The evolution and formation of a unique microstructure were further analysed by preparing the samples for cross-sectional SEM and EDX analyses. The cross-sectional image of a single-layer filling (Fig. 4e) lesion shows evidence of dislodged minerals from the interface during surface preparation using polishing. The double-layer filling (Fig. 4f) reveals that no microscopic cracks appear in the densified layer of the bio-composite, which seems to be locked around the acid-eroded surface. However, there is evidence of sub-microscopic crack formation in the adjoining enamel with each crack seeming to have been attenuated at the interface (see Fig. 4f). At around the interlocking biomimetic mineral and natural enamel interface, there appears to be a preferential segregation of iron-rich Fe-doped FAP phase. The preferential segregation of iron as phosphate suggests that the presence of this element in phosphate form aids the bonding of the biomimetic composite. The comparison of microstructures in Fig. 4e for single filling and Fig. 4f for double-layer filling shows that, in a single filler layer, the laser densification process is not as dense as in the double-layer process. This may be explained by increased energy absorption and thermal energy mediation, causing phase changes at the interface and interlocking with the natural enamel surface. The accompanying EDX map in Fig. 4g-h of the elements in the two-layer structure also confirms the presence of iron at the interface in the Fe-doped FAP mineral.

The 14-day simulated brushing trial, involving 1500 S under a 250 g applied load in an artificial saliva environment, compared the erosion resistance of natural human enamel and the restored bio-composite layer (Fig. 5). The erosion depth of natural enamel increased linearly throughout the trial, reaching approximately 14.456 µm after 1500 S. In contrast, the restored bio-composite exhibited superior wear resistance, with no visible signs of demineralisation and minimal mass loss. Specifically, the bio-composite showed only  $\sim 2~\mu m$  of material loss during the first 1000 S, after which no significant erosion was observed. The enhanced performance of the bio-composite can be attributed to its acidresistant properties, in contrast to natural enamel, which contains carbonated hydroxyapatite formed by anionic substitution in the crystal lattice [21]. This structural feature renders enamel more acid-soluble than pure hydroxyapatite, making it more susceptible to demineralisation and mechanical abrasion during brushing. These findings highlight the potential of the optimized bio-composite in mitigating erosive tooth wear under simulated oral conditions.

Primary human periodontal cells were cultured on the surface of the

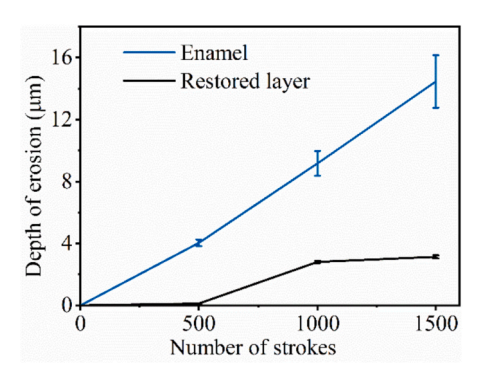


**Fig. 5.** Assessment of erosion depth following simulated tooth brushing trials conducted over 14 days, involving 1500 S under a 250 g load in an artificial saliva environment, comparing human enamel and the restored bio-composite layer (error < 5 %).

restored enamel biocomposite to evaluate biocompatibility. Both quantitative (Fig. 6d) and qualitative (Fig. 6e) cytotoxicity assessments were performed. Cellular proliferation on the biocomposite was visualized using fluorescence-based staining techniques. Cell adhesion to the biocomposite surface was further confirmed through SEM (Fig. 6a-b) and EDS (Fig. 6c). Cells were observed to grow across the bio-composite surface, exhibiting sizes ranging from approximately 10 to 30  $\mu m$ . EDS analysis validated the elemental composition of both the biocomposite and the adherent cells. The quantitative cytotoxicity was assessed using the Alamar Blue assay, which measures the reduction of resazurin to resorufin, which is a pink and fluorescent compound converted by metabolically active cells [27]. After 24 h of culture, the fluorescence intensity in the supernatant from cells grown on the biocomposite showed no statistically significant difference compared to the control group of monolayer-cultured primary periodontal cells, indicating no cytotoxicity. Qualitative cytotoxicity was evaluated using live/dead cell staining. As shown in Fig. 6e, only a small number of cells stained red with ethidium homodimer, confirming the absence of cytotoxic effects. Fluorescent staining further demonstrated cell attachment and morphology, with nuclei stained blue (DAPI) and cytoskeletal structures stained green (Fig. 6f). The cells displayed typical elongated or spindleshaped morphology [28], with clearly defined nuclei, indicating healthy proliferation and attachment on the biocomposite surface.

Further cytotoxicity analysis was performed using A549 cells with an MTT assay to evaluate the biocompatibility of the composite before and after irradiation. The material did not show any signs of cytotoxicity as compared to the control. The percentage of cell survival rate at different concentrations of bio-composite, either irradiated or non-irradiated, was calculated. The results showed that the percentage of viable cells was comparable to that of the control at different material concentrations (Fig. 7e). However, when comparing the toxicity of irradiated and non-irradiated bio-composites, it was found that the laser-irradiated bio-composite improved compatibility.

The remineralisation potential of the bio-composite was also investigated by immersing the laser-irradiated restored enamel lesion in artificial saliva. The samples were immersed in separate containers covered with aluminium foil to isolate the effect of atmospheric  $\rm CO_2$  on the saliva-induced mineralisation study. The restored enamel slabs were left at room temperature for two weeks in a saliva medium (pH 6.8). After 14 days, the restored surfaces exhibited the formation of dense, ordered rod-like mineral crystals, with nearly 100 % surface coverage as shown in Fig. 7a. EDX analysis (Fig. 7b) confirmed that the chemical composition of the remineralised layer showed a uniform distribution of calcium and phosphorus, with a Ca/P ratio of 1.72, which is close to the ratio of Ca/P in the hydroxyapatite mineral. Furthermore, the cross-sectional SEM image was analysed to confirm the thickness of the remineralised layer and its interfacial characteristics with the biocomposite. The remineralised layer formed after immersion into the

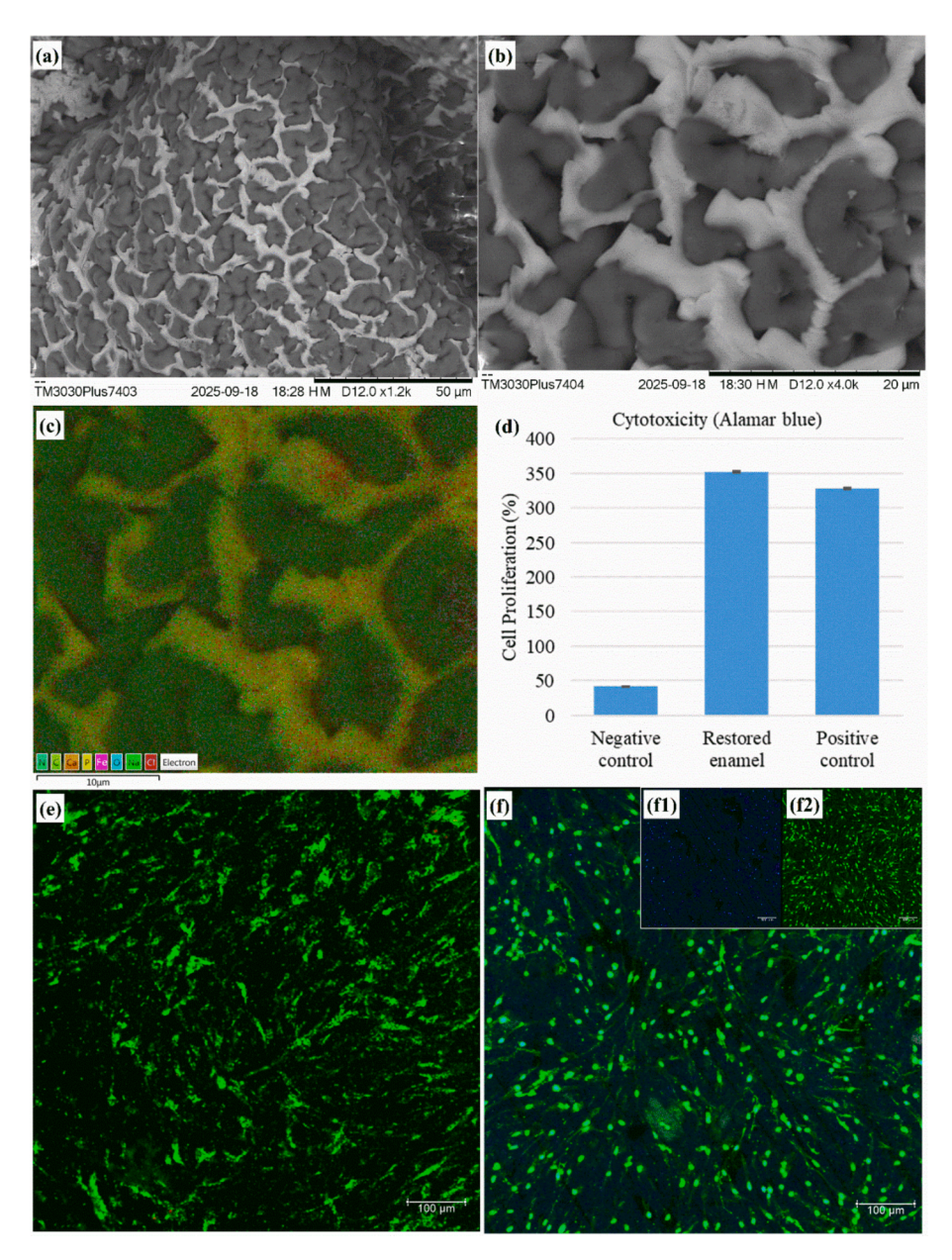


Fig. 6. Cytotoxicity evaluation of the bio-composite using periodontal cells. (a–b) SEM images showing the adhesion of human primary periodontal cells on the bio-composite coating. (c) Elemental distribution was analysed using EDS mapping. (d) Quantitative cytotoxicity assessment on restored enamel using the Alamar Blue assay. (e) Qualitative cytotoxicity analysis through live (calcein green) and dead (ethidium homodimer red) staining. (f) Confocal microscopy images illustrating nucleus and cytoskeleton organisation, with nuclei stained using blue fluorescent DAPI (f1) and cytoskeletal structures visualised using Alexa Fluor 488 (f2). The data were presented as mean value  $\pm$  SD of three separate experiments.

artificial saliva shows a well-integrated interface with the underlying bio-composite surface. The corresponding EDX map in Fig. 7d highlights the presence of the remineralised layer with a thickness of  $8.2 \pm 0.25$   $\mu m$ . It is known that chitosan can form disulfide bonds with glycoproteins. Under the specific pH and ionic strength conditions, this interaction can induce the formation of an organic–inorganic composite matrix. Additionally, it is well established in the literature that the presence of chitosan in biominerals triggers the chelation process by lowering the pH below 7, which then facilitates the modulation of pH through cellular processes (ATP/ADP) reactions, ultimately leading to a pH above 8.5. The nucleation and growth of HAP commences under these conditions, as explained in the literature [29]. These findings suggest the effectiveness of the present biomimetic approach in fabricating composite matrix materials that promote functional remineralisation.

Fig. 8 demonstrates the load-displacement curves of the nano-

indentation tests performed on the enamel, restored layer and remineralised layer. The hardness of each layer was calculated using Eq. (1).

$$H = \frac{P_{max}}{A} \tag{1}$$

where  $P_{max}$  is the maximum load applied on each layer (mN), A is the projected indentation area (nm<sup>2</sup>) and (H) is the hardness (GPa). The displacement (h<sub>max</sub>) due to the intender, recorded for each of the tested layers, for the peak load of 100 mN is summarised in Table 1. The final depth of the indentation after unloading for the enamel, restored layer and mineralised layer was recorded as 857 nm, 1722 nm and 2755 nm, respectively.

The projected area (A) for a Berkovich indenter was calculated by Eq. (2), where ( $h_c$ ) is the depth of the impression.

S. Loganathan et al. Materials & Design 260 (2025) 115151

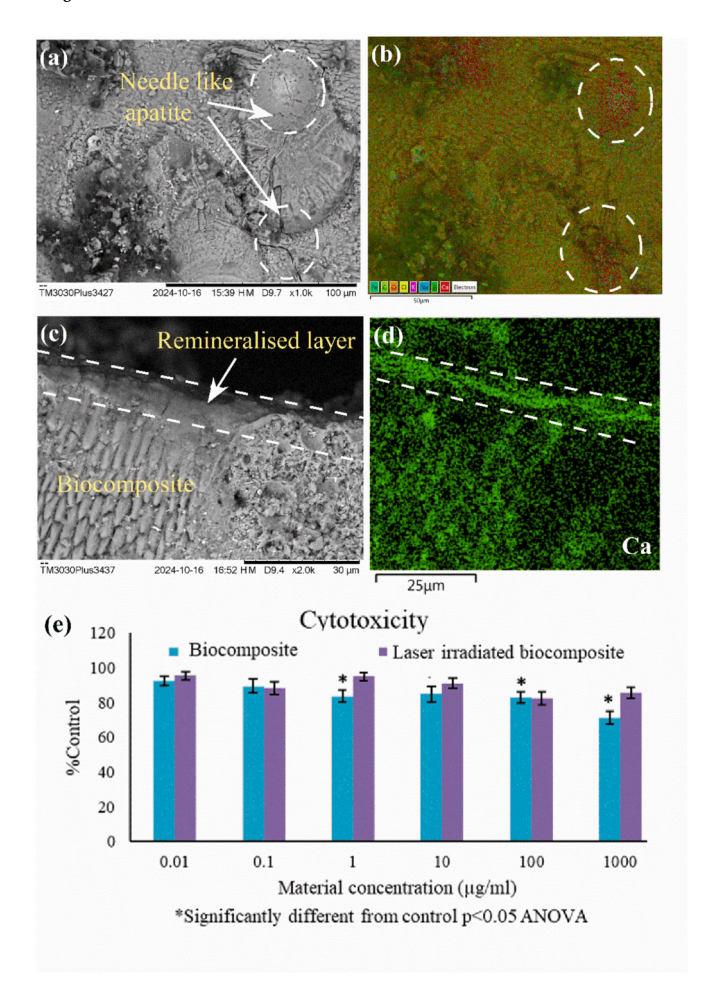


Fig. 7. Remineralisation capability of restored ETW lesion with bio-composite. (a) SEM analysis of the remineralised layer on the coating and its corresponding (b) EDX mapping. (c) Cross-sectional SEM image to evaluate the interfacial characteristics with (d) EDX. (e) Cytotoxicity-MTT analysis on bio-composite before and after irradiation.

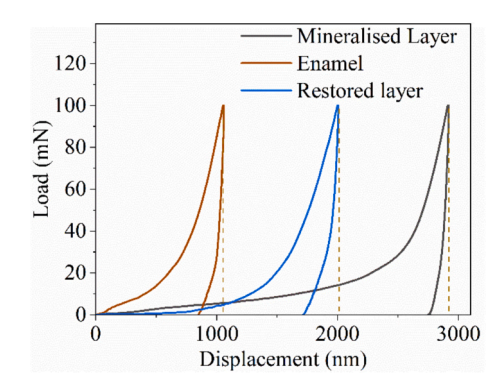


Fig. 8. Hysteresis curves from the nanoindentation analysis conducted at a  $100\,$  mN load for natural enamel, restored layer and remineralised layer.

Table 1

The max depth, final depth and hardness of enamel, restored layer and mineralised layer.

	Enamel	Restored	Mineralised
Max Depth (h <sub>max</sub> ) (nm)	1054	2010	2916
Final Depth (hf) (nm)	857	1722	2755
Hardness (GPa)	$2.87\pm0.17$	$0.74\pm0.15$	$0.21\pm0.06$

$$A = 3\sqrt{3}h_c^2 \tan^2(30) \tag{2}$$

Enamel exhibited the highest hardness (2.87  $\pm$  0.17) GPa when compared to the restored defect (0.74  $\pm$  0.15) GPa and the mineralised layer (0.21  $\pm$  0.06) GPa. The restored layer presented hardness comparable to restorative materials such as micro hybrid resins and nanofiller resins (0.7 GPa) and human bone (0.59 GPa) [30]. The hardness of the enamel and restored layer are comparable to previously conducted research [21]. Any deviations in the layer hardness (17 %) were attributed to potential variations in the thickness and morphology of the applied coating.

The Raman analysis was performed to further investigate the newly formed mineral layer on the restored enamel samples (Fig. 9). The raw Raman data were normalised using Fityk software. The phosphate (PO $_4^3$ ) vibration bands confirmed the presence of apatite (restored dental enamel immersed in artificial saliva) which is precipitated between Day 0, Day 7, and Day 14 are represented by the Raman spectra (Fig. 6). These intense vibration bands are termed  $\nu_1 PO_4^3$  (~960 cm $^{-1}$ ),  $\nu_2 PO_4^3$  (~430 cm $^{-1}$ ), and  $\nu_4 PO_4^3$  (~590 cm $^{-1}$ ), which represent phosphate stretching and bending modes. The  $\nu_1 PO_4^3$  symmetric stretching band exhibits a wavenumber increase and progressively increasing intensity over time, reflecting higher crystallinity and more tightly packed ions in the apatite lattice due to exposure to the salivary environment. Binding interactions with salivary ions such as Ca $^{2+}$ , PO $_4^3$ , and OH $_1$  would stabilise the bonding geometries, leading to a higher frequency shift.

With this, deconvoluted Raman peaks further confirm that on Day 0, the less intense and broader profile of  $\nu_1$  at  $\sim$  958 cm<sup>-1</sup> validates the greater amorphous content (Fig. 9). At Day 7, the peak increased but shifted towards 960 cm<sup>-1</sup>, signifying the commencement of crystal growth. At Day 14, it is significantly restricted and increased in strength, reaching approximately 962 cm<sup>-1</sup> resulting in greater structural ordering and mineral maturity. The shoulder peak at around 945 cm<sup>-1</sup>, which is stronger at an earlier stage, is attributed to amorphous calcium

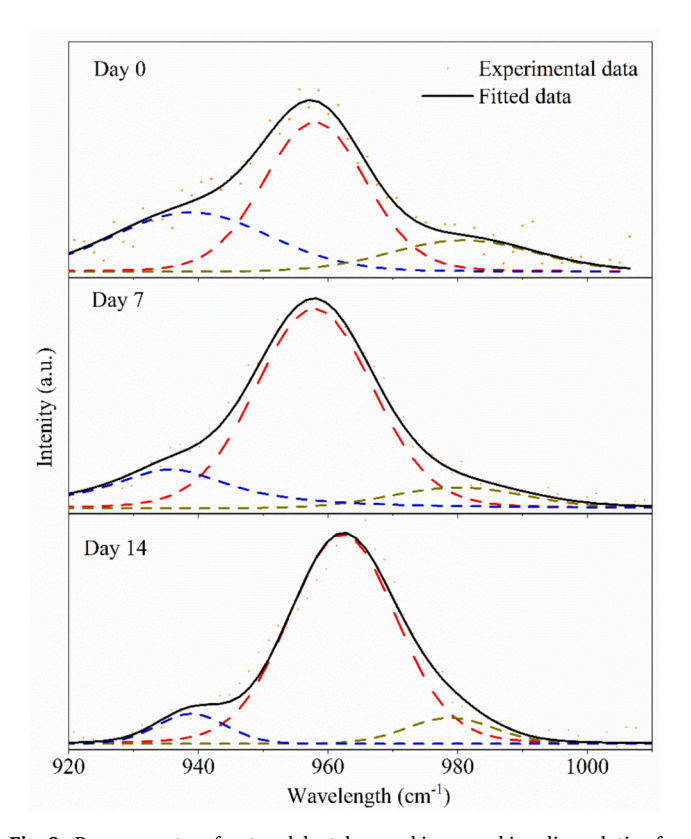


**Fig. 9.** Raman spectra of restored dental enamel immersed in saliva solution for different time intervals.

S. Loganathan et al. Materials & Design 260 (2025) 115151

phosphate and reduces with increasing mineralisation time. Meanwhile, a low-intensity peak at around 975 cm $^{-1}$  can be attributed to a second phase of carbonate or phosphate substitution. In addition, the  $\nu_2 PO_4^{3-}$  and  $\nu_4 PO_4^{3-}$  bending bands are reasonably enhanced by Day 14, thus showing structural solidity and formation of mineral density. The spectral and intensity changes of phosphate vibrational bands are evidence of effective remineralisation, structural maturity, and apatite stability in a salivary medium mimicking natural biomineralisation, such as bone and dental tissues.

The XRD analysis (Fig. 10) reveals the gradual maturation of the mineral over the enamel which was subjected to restoration and remineralization treatments. The  $2\theta$  angles around  $26^{\circ}$  and  $32^{\circ}$ , belonging to the (0 0 2) and (2 1 1)/(3 0 0) planes of hydroxyapatite (HAp), are clearly visible in all the patterns, and thus, it is confirmed that apatite is the dominant mineral phase over the whole range of natural, restored, and remineralised samples. The natural enamel shows strong and sharp peaks which are the sign of a highly crystalline, well-ordered apatite lattice that is characteristic of mature dental tissue. On the contrary, the restored layer presents the same characteristic peaks but with moderate intensity and slight broadening which might be due to the presence of apatite with smaller crystallite size and lower structural order than that of natural enamel. The remineralised layer has the broadest and the least intense peaks which corresponds to a poorly crystalline apatite or amorphous calcium phosphate (ACP) formed during the early stages of mineral deposition is present there. There are no additional diffraction peaks detected, which confirmed that the mineral layer remains phasepure and free of secondary crystalline impurities. It can be concluded that saliva-mediated ion exchange leads to mineral nucleation and subsequent crystal growth which results in lattice order and crystallinity increase over time. This structural evolution revealed by XRD confirms perfectly the results obtained from Raman spectroscopy. The  $\nu_1$  PO<sub>4</sub><sup>3-</sup> stretching band at  $\sim 958 \text{ cm}^{-1}$  on Day 0 shifts to  $\sim 962 \text{ cm}^{-1}$  on Day 14, and this is accompanied by peak narrowing and intensity enhancement which are indicative of the formation of stronger phosphate bonds and tighter lattice packing.

### 3.3. In-situ evaluation of restored dental enamel

Building on the promising in-vitro experimental results, an in-situ

human study was designed (section 2.6), where we evaluated the clinical performance of the bio-composite coating for the ETW. The optical microscopic images of single-layer and double-layer coatings reveal that the biomimetic coating remained intact (Fig. 11c-d) in the in-situ oral environment during the experimental period, ensuring the integrity of the bio-composite over the enamel surface.

A lesion depth of  $\sim 70 \, \mu m$  was introduced in the 22 test enamel blocks. However, a total lesion depth of  $\sim 95 \, \mu m$  was observed in the samples. The increase in lesion  $(oral control - control = 25 \mu m, Fig. 11a-b)$  was attributed to mineral loss occurring in the oral environment. Group (1) samples restored with a single-layer bio-composite averaged a lesion depth of  $\sim 61~\mu m$ (Fig. 11a), whereas Group 2 samples restored with a double-layer biocomposite exhibited a lesion depth of  $\sim$  36 µm (Fig. 11b). Single-layered composite also observed an increase in lesion depth (~33 µm) after exposure to the oral environment, followed the similar pattern of mineral loss. However, the double-layered samples exhibited less mineral loss compared to the single-layer samples. Double-layer surface mineral loss is comparable to that of the controls, suggesting that double-layer restoration could mimic the natural characteristics of dental tissue. The observed interfacial characterisation and microstructural rearrangement of minerals in double-layered bio-composite (Fig. 4f) restoration could explain its efficiency in ETW resistance.

The lesion restored with a single-layer bio-composite (oral singlelayer, Fig. 11a) did not show a statistically significant reduction in lesion depth compared to the oral control (p > 0.203). However, this result should be interpreted with caution. The estimated effect size (Cohen's d = -0.347) was small, and the 95 % confidence interval [-1.171, 0.477] included zero, indicating substantial uncertainty. Furthermore, the statistical power was low (0.125), suggesting the study may have been underpowered to detect a meaningful difference. In contrast, the double-layer bio-composite coating (oral double-layer, Fig. 11b) demonstrated a statistically significant reduction in lesion depth (p < 0.0001) compared to the oral control. These findings suggest that the double-layer repair technique may offer more effective prevention of erosive tooth wear (ETW) than the single-layer approach, though further studies with larger sample sizes are needed to confirm the clinical relevance of the single-layer method. In order to address this limitation, a large-scale in situ human study is being planned, involving

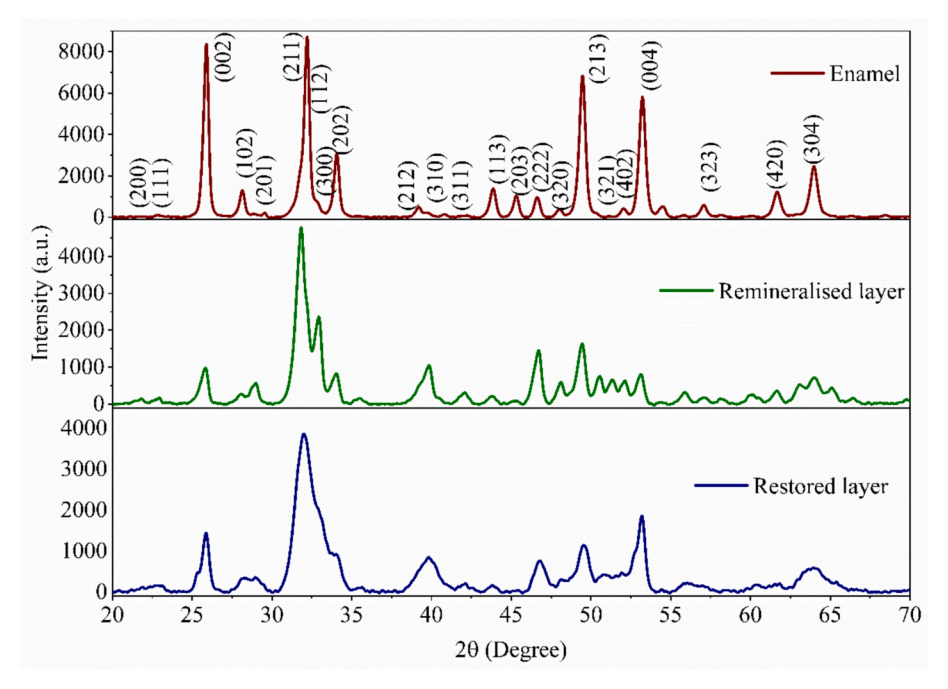


Fig. 10. XRD pattern of sound enamel, restored layer with bio-composite and remineralised layer following 14 days of immersion in artificial saliva.

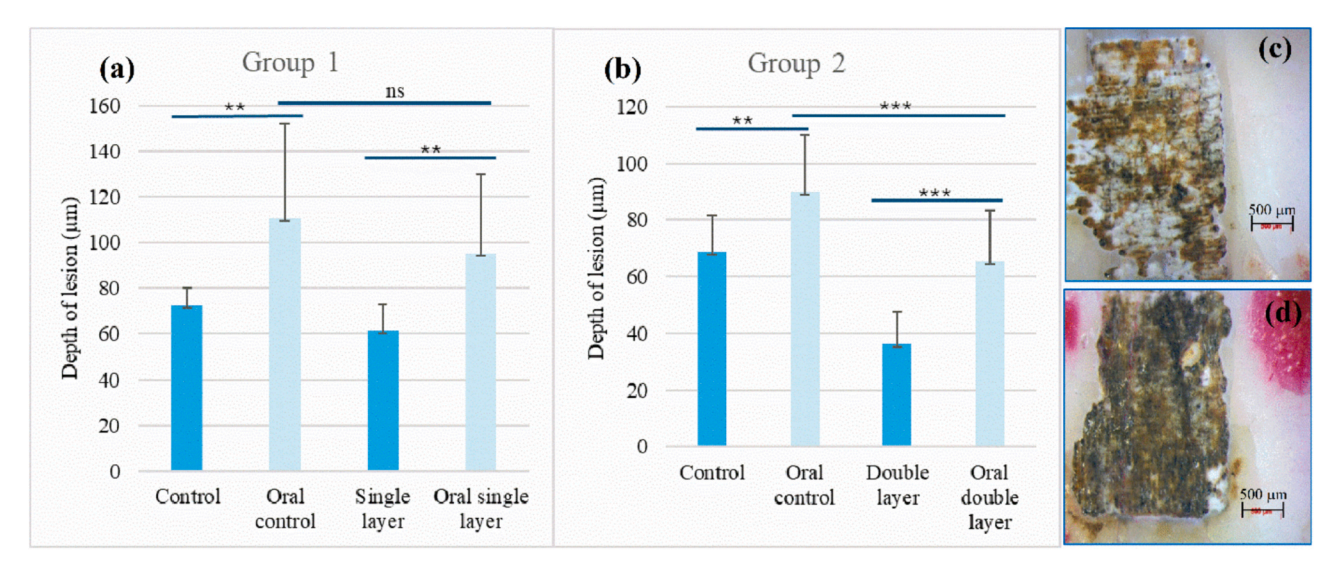


Fig. 11. Assessment of lesion depth in control versus repaired enamel slabs before and after the in-situ study for (a) single-layer and (b) double-layer of composites. The statistical significance is denoted as follows:  $p < 0.05 \rightarrow *, p < 0.01 \rightarrow ***, p < 0.001 \rightarrow ****. Optical microscopic image of (c) single layer and (d) double layer composite coating after in-situ study.$ 

approximately 100 participants from various locations across the UK.

#### 4. Proposed translational path for the future

The data from early-stage preclinical research has demonstrated a path for restoring tooth surface loss, demonstrating the application of a near-IR 1040 nm ultrafast laser in combination with a photo-absorptive bio-composite. The synthesis and characterisation of bio-composites for enamel restoration were optimised along with the laser parameters required for restorative procedures in vitro. The samples were then prepared for in-situ mouth appliance trials with healthy volunteers. The combination of organic and inorganic mineral composition in the proposed bio-composite reflecting hard tissue composition when treated with an ultra-precision laser might be suggestive of an appropriate restorative material suitable for handling in a challenging oral environment. The suggestive findings of this study pave the way for exploring a potential restorative technique to restore the highly prevalent dental erosive lesions, such as ETW. Achieving precise enamel restoration might require an optimised inertial robotic system equipped with vision sensors capable of treating sub-millimetre lesions.

# 5. Conclusions

The present study proposed a technique for the direct dental restoration of ETW using ultrafast laser-assisted bio-composite coatings. The chitosan-based bio-composite exhibited potential for remineralisation by forming an organic-inorganic composite matrix. In-vitro results demonstrated that the bio-composite coating effectively promoted remineralisation on the restored dental surface. Statistical analysis of the in-situ study indicated that the double-layer coating was significantly more effective than a single-layer application. These findings suggest that laser-assisted biomimetic composite coatings might serve as a template for inducing biomineralisation, offering a promising therapeutic strategy for arresting and preventing erosive tooth wear.

# CRediT authorship contribution statement

**Sarathkumar Loganathan:** Writing – original draft, Validation, Project administration, Methodology, Formal analysis, Data curation, Conceptualization. **Sandeep Kumar:** Writing – review & editing, Validation, Software, Formal analysis, Data curation. **Simon Strafford:** Visualization, Resources, Methodology. **Geeta Sharma:** Writing –

review & editing, Validation, Software, Formal analysis, Data curation. **Evangelos Daskalakis:** Resources, Investigation, Formal analysis, Data curation. **Eric Kumi Barimah:** Resources, Methodology, Formal analysis. **Neelam Iqbal:** Visualization, Resources. **Anna Neilson:** Resources, Project administration, Investigation, Formal analysis. **Brian Nattress:** Validation, Software, Resources, Investigation. **Sue Pavitt:** Visualization, Supervision, Resources, Data curation. **El M Raif:** Writing – review & editing, Resources, Methodology, Data curation. **Animesh Jha:** Writing – review & editing, Supervision, Project administration, Investigation, Funding acquisition, Conceptualization.

# Declaration of competing interest

The authors declare that they have no known competing financial interests or personal relationships that could have appeared to influence the work reported in this paper.

### Acknowledgements

The authors acknowledge the financial support from the European Union's Horizon 2020 Research and Innovation (NMBP) Programme under Grant Agreement No. 953128, UKRI EPSRC grant reference numbers. EP/N00941X/1 and EP/K020234/1. The authors gratefully acknowledge the clinical support and guidance provided by Dr. Graeme Howling (Medipex, York, UK) and Prof. M. S. Duggal (College of Dental Medicine, Qatar University, Doha, Qatar) for their recommendations regarding volunteers for the in-situ mouth appliance study.

# Data availability

Data will be made available on request. However, due to the sensitive nature of the in-situ human study, any questions related to patients' data would remain confidential and would not be shared

#### References

- S. Kalyani, B.A. Reginald, B.S. Reddy, M. Samatha, Dental erosion-an occupational hazard among battery manufacturing industry workers in Hyderabad, India,, Ind. J. Occup. Environ. Med. 28 (2024) 41–44, https://doi.org/10.4103/ijoem.ijoem\_ 85.23
- [2] F. Inchingolo, G. Dipalma, D. Azzollini, I. Trilli, V. Carpentiere, D. Hazballa, I. R. Bordea, A. Palermo, A.D. Inchingolo, A.M. Inchingolo, Advances in preventive and therapeutic approaches for dental erosion: a systematic review, Dent. J. (basel) 11 (2023), https://doi.org/10.3390/dj11120274.

- [3] L.C. De Lima, K. Landmayer, M.M. Braga, Tain. Scaramucci, R.G. Palma-Dibb, Effect of laser irradiation associated with fluoride in decreasing erosive tooth wear: a systematic review with a network meta-analysis, Journal of Evidence-Based Dental Practice 24 (2024). https://doi.org/10.1016/j.jebdp.2024.101990.
- [4] S. Loganathan, G. Sharma, E. Daskalakis, S. Strafford, E. Kumi Barimah, A. Jha, Ultrashort pulsed laser-assisted direct restoration of human enamel using 3D printable biocomposite,, Adv. Mater. Technol. 10 (2025), https://doi.org/ 10.1002/admt.202401362.
- [5] G. Campus, J.Y. Niu, B. Sezer, O.Y. Yu, Prevention and management of dental erosion and decay, BMC Oral Health. 24 (2024), https://doi.org/10.1186/s12903-024-04257-y.
- [6] N. Schlueter, B. Luka, Erosive tooth wear a review on global prevalence and on its prevalence in risk groups, Br. Dent. J. 224 (2018), https://doi.org/10.1038/sj. bdi.2018.167.
- [7] P. Huang, Q. Nie, Y. Tang, S. Chen, K. He, M. Cao, Z. Wang, A novel nerol-segmented waterborne polyurethane coating for the prevention of dental erosion, RSC Adv. 14 (2024) 16228–16239, https://doi.org/10.1039/d4ra01744g.
- [8] Y. Pang, C. Fu, D. Zhang, M. Li, X. Zhou, Y. Gao, K. Lin, B. Hu, K. Zhang, Q. Cai, P. Yang, Y. Liu, X. Zhang, Biomimetic remineralization of dental hard tissues via amyloid-like protein matrix composite with amorphous calcium phosphate, Adv. Funct. Mater. (2024), https://doi.org/10.1002/adfm.202403233.
- [9] F. Marro, S. De Smedt, S. Rajasekharan, L. Martens, P. Bottenberg, W. Jacquet, Associations between obesity, dental caries, erosive tooth wear and periodontal disease in adolescents: a case-control study, Eur. Arch. Paediatr. Dent. 22 (2021) 99–108, https://doi.org/10.1007/s40368-020-00534-w.
- [10] N. Iqbal, T.M. Braxton, A. Anastasiou, E.M. Raif, C.K.Y. Chung, S. Kumar, P. V. Giannoudis, A. Jha, Dicalcium phosphate dihydrate mineral loaded freeze-dried scaffolds for potential synthetic bone applications, Materials 15 (2022), https://doi.org/10.3390/ma15186245.
- [11] G. Sharma, S. Loganathan, E.K. Barimah, P. Georgopoulou, E. Taylor, A.J. Scott, S. Strafford, A. Jha, Effect of rare earth ion substitution on phase decomposition of apatite structure, ChemPhysChem 25 (2024), https://doi.org/10.1002/ cphc.202400109.
- [12] G. Sharma, S. Loganathan, E. Daskalakis, E.K. Barimah, S. Strafford, A. Jha, Phase stability in rare-earth-doped apatites: a machine learning approach, Adv. Intell. Syst. (2025), https://doi.org/10.1002/aisy.202500293.
- [13] R.H.A. el-baky, H.A. Adawy, N.A.M. Ahmed, Biomimetic dentin remineralization via chitosan hydrogel versus recaldent paste. (an in vitro study),, Al-Azhar J. Dent. 11 (2024), https://doi.org/10.58675/2974-4164.1629.
- [14] Z. Zhang, Z. Cui, J. Zhang, H. Zheng, Z. Zhou, Z. Wu, Z. Wang, B. Fu, Remineralizing effects of hydroxypropyl methylcellulose film-loaded amorphous calcium phosphate nanoprecursors on enamel artificial caries lesions, J. Mech. Behav. Biomed. Mater. 151 (2024), https://doi.org/10.1016/j. imbbm.2024.106408.
- [15] S. Loganathan, S. Santhanakrishnan, R. Bathe, M. Arunachalam, FTIR and Raman as a noninvasive probe for predicting the femtosecond laser ablation profile on heterogeneous human teeth, J. Mech. Behav. Biomed. Mater. 115 (2021), https:// doi.org/10.1016/j.jmbbm.2020.104256.
- [16] E. Daskalakis, A. Scott, R. Mangham, N. Middleton, A. Jha, Laser ignition chemical synthesis of bulk Al<sub>2</sub>O<sub>3</sub>-TiB<sub>2</sub> composites for impact resistance application, J. Mater. Res. Technol. 38 (2025) 6063–6082, https://doi.org/10.1016/j.jmrt.2025.09.045.
- [17] S. Loganathan, S. Santhanakrishnan, R. Bathe, M. Arunachalam, Physiochemical characteristics: a robust tool to overcome teeth heterogeneity on predicting laser

- ablation profile, J. Biomed. Mater. Res. B Appl. Biomater. 109 (2021) 486–495, https://doi.org/10.1002/jbm.b.34717.
- [18] K.P. Chang, T.W. Tsai, K.Y. Huang, C.H. Huang, S.Y. Wang, C.W. Cheng, J.K. Chen, D.Y. Tzou, Thermal response of a dental tissue induced by femtosecond laser pulses, Appl. Opt. 52 (2013) 6626–6635, https://doi.org/10.1364/AO.52.006626.
- [19] E. Daskalakis, N. Iqbal, S. Loganathan, E. Spettoli, G. Morozzi, A. Ballardini, P. V. Giannoudis, A. Jha, Effect of laser drilling on biomorphically engineered hydroxyapatite scaffolds derived from rattan wood, Mater. Des. 245 (2024), https://doi.org/10.1016/j.matdes.2024.113243.
- [20] H.H. Casarin, V.S. Mattos, J.C. de Castro Neto, M.A. Chinelatti, Chemical and morphological changes of femtosecond laser-irradiated enamel using subablative parameters, Microsc. Res. Tech. 84 (2021) 2399–2408, https://doi.org/10.1002/ iemt\_23795
- [21] A.D. Anastasiou, S. Strafford, C.L. Thomson, J. Gardy, T.J. Edwards, M. Malinowski, S.A. Hussain, N.K. Metzger, A. Hassanpour, C.T.A. Brown, A. P. Brown, M.S. Duggal, A. Jha, Exogenous mineralization of hard tissues using photo-absorptive minerals and femto-second lasers; the case of dental enamel, Acta Biomater. 71 (2018) 86–95, https://doi.org/10.1016/j.actbio.2018.02.012.
- [22] A.D. Anastasiou, C.L. Thomson, S.A. Hussain, T.J. Edwards, S. Strafford, M. Malinowski, R. Mathieson, C.T.A.A. Brown, A.P. Brown, M.S. Duggal, A. Jha, Sintering of calcium phosphates with a femtosecond pulsed laser for hard tissue engineering, Mater. Des. 101 (2016) 346–354, https://doi.org/10.1016/j. matdes 2016 03 159
- [23] B.T. Amaechi, S.M. Higham, W.M. Edgar, The use of gamma irradiation for the sterilization of enamel for intra-oral cariogenicity tests, J. Oral Rehabil. 26 (1999) 809–813, https://doi.org/10.1046/j.1365-2842.1999.00460.x.
- [24] S.J. Evans, R.L. Lawrence, M. Ilett, M.J. Burgum, K. Meldrum, N. Hondow, G. J. Jenkins, M.J.D. Clift, S.H. Doak, Industrial-relevant TiO<sub>2</sub> types do not promote cytotoxicity in the A549 or TK6 cell lines regardless of cell specific interaction, Toxicol. In Vitro 83 (2022), https://doi.org/10.1016/j.tiv.2022.105415.
- [25] M. Bonany, A.J. Pérez-Berná, T. Dučić, E. Pereiro, H. Martin-Gómez, C. Mas-Moruno, S. van Rijt, Z. Zhao, M. Espanol, M.P. Ginebra, Hydroxyapatite nanoparticles-cell interaction: new approaches to disclose the fate of membrane-bound and internalised nanoparticles, Biomat. Adv. 142 (2022), https://doi.org/10.1016/j.bjoadv.2022.213148
- [26] G.L. Hovis, B.T. Scott, C.M. Altomare, A.R. Leaman, M.D. Morris, G.P. Tomaino, F. M. McCubbin, Thermal expansion of fluorapatite-hydroxylapatite crystalline solutions, Am. Mineral. 99 (2014) 2171–2175, https://doi.org/10.2138/am-2014-4014
- [27] S.N. Rampersad, Multiple applications of alamar blue as an indicator of metabolic function and cellular health in cell viability bioassays, Sensors (switzerland) 12 (2012) 12347–12360, https://doi.org/10.3390/s120912347.
- [28] M. Köunönen, M. Hormia, J. Kivilahti, J. Hautaniemi, I. Thesleff, Effect of surface processing on the attachment, orientation, and proliferation of human gingival fibroblasts on titanium, J. Biomed. Mater. Res. 26 (1992) 1325–1341, https://doi. org/10.1002/jbm.820261006.
- [29] D. Raafat, H.G. Sahl, Chitosan and its antimicrobial potential a critical literature survey, Microb. Biotechnol 2 (2009) 186–201, https://doi.org/10.1111/j.1751-7915.2008.00080.x.
- [30] P.K. Zysset, X.E. Guo, C.E. Hoffler, K.E. Moore, S.A. Goldstein, Elastic modulus and hardness of cortical and trabecular bone lamellae measured by nanoindentation in the human femur, J. Biomech. 32 (1999) 1005–1012, https://doi.org/10.1016/ S0021-9290(99)00111-6.